Fabrication of opaque aluminum electrode-based perovskite solar cells enabled by the interface optimization

Xue Sun [a,b,c], Tong Lin [a], Changzeng Ding [a], Shuxuan Guo [a], Irfan Ismail [a], Zhenguo Wang [a], Junfeng Wei [a], Qun Luo [a], Jian Lin [a], Dongyu Zhang [a,**], Chang-Qi Ma [a,*]

[a] *Printable Electronics Research Center, Suzhou Institute of Nano-Tech and Nano-Bionics, Chinese Academy of Sciences, 398 Ruoshui Road, SEID, SIP, Suzhou, 215123, PR China*
[b] *Guangzhou Institute of Measurement and Testing Technology, GuangZhou, 510640, PR China*
[c] *School of Mechanical and Automotive Engineering, South China University of Technology, Guangzhou, 510640, PR China*

ARTICLE INFO

ABSTRACT

In the total cost of perovskite solar cells (PVSK), the most successfully used indium-tin-oxide (ITO) transparent electrode takes up a substantial amount, which could be big limit for the commercialization of PVSK cells. Aluminum (Al) foil is an extremely low-cost metal electrode with high conductivity and is an ideal alternative for the ITO electrode in PVSKs. Aiming to develop low-cost PVSK, we systematically optimized the layer sequential of inverted PVSK based on the opaque Al bottom electrode. The unsuitable work functions of Al electrode and the poly(bis(4-phenyl)(2,4,6-trimethylphenyl)amine (PTAA) hole transport layer lead to low device performance. Through the introduction of a thin molybdenum (VI) oxide (MoO$_3$) layer between the Al electrode and PTAA layer, the hole injection barrier was minimized, leading to a dramatic improvement of device performance. By adjusting the thicknesses of the MoO$_3$ interlayer, a champion cell showed a power conversion efficiency of 7.09% based on spray-coated silver nanowires top electrode, proving the concept of using aluminum foil in making low-cost perovskite solar cells.

1. Introduction

The development of perovskite solar cell (PVSK) has entered a golden age since the first reported by Miyasaka et al. in 2009 [1]. The power conversion efficiency (PCE) has rapidly increased from 3.8% to a remarkable number of over 25% [2]. Perovskite film, the indispensable part of perovskite solar cells, are generally prepared from lead halides and organic ammonium salts, which are cheap and earth's crust contain enough materials [3–5]. In combination with the solution processability of various functional layers, perovskite solar cells are expected to be low-cost and drawn enormous attention both from the academy research and industry communities.

In a complete perovskite solar cell, both the top and bottom electrodes are essential layers. Transparent conductive oxides (TCO), such as indium-tin-oxide (ITO) and fluorine-doped tin oxide (FTO) are the most widely used bottom electrode owing to their balanced conductivity and transparency [6–8], whereas opaque metal electrode, such as aluminum (Al), silver (Ag) and gold (Au) are used as the top electrode, which are usually prepared by vacuum deposition methods [9–11]. Although TCO is widely used as the bottom electrode, TCOs are rarely used as top electrode owing to its complicated deposition processes [12–14]. In addition, TCO electrodes suffer from brittle nature as well as high fabrication costs [15]. For example, Chang et al. showed that ITO bottom electrode and gold top electrodes take up over 70% of the total cost in PVSK devices [16]. To meet these challenges, researchers have developed various potentially low-cost alternative transparent conductors as the electrode for perovskite solar cells, such as carbon-based materials [17–20], conductive polymers [21–23], metal foils [24,25] and metal nanowires [26,27]. With these, the fabrication of perovskite solar cells from the opaque metal electrode became possible. Peng firstly reported the integration of perovskite solar cells into a flexible fiber, in which stainless steel and carbon nanotubes were used as the bottom and top electrode, respectively [28]. Following this, perovskite solar cells based on Ti [25,29–34], Cu foil [24], as well as Ag electrode [35,36] were reported, where carbon nanotube [36], ultra-thin metal films [25, 30,36], TCO [32,34], conductive polymer [31,35], and silver nanowires

---

(AgNWs) [24,33] were used as the transparent top electrode, and PCE of 6–15% were reported for these cells.

Al has the advantages of extra low-cost, high conductivity, and suitable work function (WF, −4.28 eV) [37] for both hole [38–40] and electron [41–43] collection in solar cells, and these superiorities make Al a promising bottom electrode for perovskite solar cells. However, there is no report on the perovskite solar cells using Al as the bottom electrode. Recently, we have successfully prepared silver nanowires based transparent electrode for use organic [44,45] and perovskite solar cells [46, 47], where highly transparent and conductive AgNW electrode were prepared either by ink-jet printing or spray-coating. We therefore proposed to prepare perovskite solar cells from Al bottom electrode with solution-processed AgNW top electrode, which should be able to reduce the cost of the perovskite solar cells dramatically. Aiming to this, we report the preparation of structure inverted perovskite solar cells based on opaque Al bottom electrode and spray-coated AgNW top transparent electrode. To eliminate the negative solvent effect during the spray coating of AgNW electrode, we firstly use thermally evaporated ultra-thin Ag film as the top electrode to optimize the interfacial connection between Al bottom electrode and the organic hole transporting layer poly(bis(4-phenyl)(2,4,6-trimethylphenyl)amine (PTAA). Surprisingly, we found that hole injection between PTAA and Al electrode is poor owing to the mismatched energy levels. Through the introduction of a thin molybdenum (VI) oxide (MoO_3) layer, the charge injection barrier was minimized, which leads to the significant improvement of device performance. Based on the optimized interfacial connection, for the first time, we successfully prepared perovskite solar cells based on opaque Al bottom electrode and spray-coated AgNW top electrode, which show a potentially low cost.

2.   . Experimental section

2.1. Materials

Patterned ITO glass was purchased from Shenzhen South China Xiangcheng Technology Co., Ltd. MoO_3 powder (99.999%-Mo) was purchased from Strem Chemicals, Inc. High purity aluminum particle was purchased from Zhongnuo Advanced Material (Beijing) Technology Co. Ltd. The PTAA, $PbCl_2$ (99%), Methylammonium Iodide (CH_3NH_3I) (99.5%) and PbI_2 (99%) were all purchased from Xi'an Polymer Light Technology Corp. Phenyl-C_{61}-butyric acid methyl ester ($PC_{61}BM$) was provided by Solarmer Energy, Inc. (Beijing). Branched poly-ethyleneimine (PEI, Mn $= 2.5 \times 10^4$ g mol^{-1}) was purchased from Sigma Aldrich. The AgNWs water dispersion with a concentration of 10 mg mL^{-1} was purchased from Nanchang H&C Advanced Materials Co. Ltd. The high concentration of AgNWs dispersion was diluted with a certain amount of water and isopropanol (IPA) with a ratio of 1:4. The final concentration of AgNWs dispersion is 1.2 mg mL^{-1}.

2.2. Fabrication of perovskite solar cells based on Al and ITO bottom electrode

For Al-based PVSK devices, thin glass was used as substrates. The glass substrates were cut into 2.5 × 2.5 cm^2 and then sequentially cleaned by deionized water, acetone, and IPA to remove surface impurities. After completely drying the substrates, Al electrodes were patterned deposited with the vacuum thermal evaporation technique at a pressure of 6×10^{-4} Pa. For MoO_3 modified devices, various thicknesses MoO_3 were deposited on Al electrodes also with vacuum thermal evaporation technique after the Al evaporation. PTAA was dissolved in toluene with a concentration of 2.2 mg mL^{-1} and ultrasonically treated for 2 h. The fully dissolved PTAA solution was spin-coated directly on Al or MoO_3 modified Al bottom electrodes at 5000 revolutions per minute (rpm) for 50 s, then followed by thermal treating at 105 °C for 5 min. After PTAA hole transport layer cooled down to room temperature, 0.5 mg mL^{-1} PEI dissolved in IPA was spin-coated on it at 3000 rpm for 50s

and then thermally annealed at 105 °C for 5 min to increase the wettability of the upper interface layer. The perovskite precursor solution was prepared by mixing 103.35 mg CH_3NH_3I, 306.56 mg PbI_2, and 9.73 mg $PbCl_2$ in a mixture solvent of 350 μL Gamma-butyrolactone and 150 μL dimethylsulfoxide. The precursor solution was stirred at 55 °C overnight before use. The perovskite layer was fabricated through an anti-solvent procedures described below [48]: 50 μL perovskite precursor solution was dropped onto PEI modify layer at 1000 rpm for 10 s and then 4000 rpm for 30 s. During the spinning processing, 450 μL chlorobenzene (CB) was added onto the substrate at the 17th second. The yellowish perovskite precursor film was then thermally annealed at 100 °C for 10 min to fully convert into dark brown perovskite film. $PC_{61}BM$ was dissolved in CB with a concentration of 20 mg mL^{-1} and ultrasonically treated for 2 h. After the dark brown perovskite film cooled down to room temperature, a fully dissolved $PC_{61}BM$ solution was spin-coated on it at 1000 rpm for 45s to form an electron transport layer. For the PVSKs using spray-coated AgNWs or evaporated thin Ag conductive film as top electrodes, 1 mg mL^{-1} PEI dissolved in IPA was spin-coated onto $PC_{61}BM$ film at 5000 rpm for 60s to improve the connection and minimize the charge injection barrier between $PC_{61}BM$ and top electrodes [47].

For devices with evaporated thin Ag (e-Ag) as top electrodes, after spin-coated PEI interface layers, 12 nm thin Ag layers were thermal evaporated through a shadow mask at a pressure of about 6×10^{-4} Pa. For devices with spray-coated AgNWs as top electrodes, the AgNWs dispersion was spray-coated on top of PEI interface layer with a spray coater (Hizenith AC300-1, Hizenith Robot (Suzhou) Co., Ltd.), the nozzle moving speed was 16 mm s^{-1}. The substrates were kept on a hotplate of 53 °C during the spray-coating process in order to speed up the evaporation of dispersants. Finally, AgNWs electrodes with AgNWs density of 6.2 μg cm^{-2}, averaged sheet resistance of 27.0 Ω □$^{-1}$ and an averaged light transparence (AVT) of 91% could be obtained. After the deposition of AgNWs electrode, the solar cells were annealed at 85 °C for 5 min.

For PVSK based on ITO, patterned ITO glasses were first cleaned as the glass substrates mentioned above. After completely drying the ITO glasses, other interface layers were fabricated in the same way as the devices based on metal electrodes. The active areas of these perovskite solar cells with different electrodes are all 0.04 cm^2 defined by a photomask for solar simulator measurements.

2.3. Characterization of films

The film thicknesses in this report were measured by a step profiler (Veeo, Dektak 150). After the deposition of film to be tested, the probe gently slides along the film surface and moves up and down along the surface peaks and valleys, this movement of the probe reflects the surface profile. The conductive films' sheet resistances were measured by a four-point probe station (Suzhou Jingge ElectronicCo., Ltd)). The light transparency of the electrodes, including spray-coated AgNW films and thermal-evaporated thin Ag films, were measured using a UV–visible spectrometer (Lambda 750, PerkinElmer).

2.4. Characterization of device

The current density-voltage (*J-V*) characters of the perovskite solar cells under a simulated sun AM 1.5 G (Newport VeraSol-2 LED Class AAA Solar Simulator) were measured with a Keithley 2400 source meter. All these PVSK devices were top-illuminated. The external quantum efficiencies (EQE) were tested by a home-made system, which has a 150 W tungsten halogen lamp (Osram 64642) as the light source, a monochromator (Zolix, Omni-l300) to get the monochromic light, an I–V converter (QE-IV Convertor, Suzhou D&R Instruments) and a lock-in amplifier (Stanford Research Systems SR 830) to record the photon-to-electronic response.

3. Result and discussion

3.1. Preparation and characterization of Al and Al/MoO₃ composite electrodes

Al has been commonly used as the cathode in perovskite thin-film solar cells [49–52]. For its low WF of −4.28 eV, Al is not an appropriate choice as the anode for thin-film solar cells. To minimize the hole injection barrier from the photoactive layer to the Al anode, we introduce a high WF interfacial layer between the photoactive layer and the Al anode [53]. Metal oxide interface layers have been proved to have great capability to tune the WF of metallic electrodes by adsorption, charge transfer and reaction [54]. Among the family of metal oxide materials, MoO_3 has been recognized as the ideal hole transporting layer materials in photoelectric devices, owing to its low-lying electronic state (WF of −5.6 eV) and the strong n-doped by oxygen vacancies [55,56]. For this reason, a thin MoO_3 layer was introduced to modify the Al electrode, and the properties of Al and Al/MoO_3 electrodes were then systematically investigated.

It is well known that the wettability greatly influences the film-forming capability for the deposition of the functional layers via solution processing. The improved adhesion also contributes to reducing the electrical contact resistance in the vertical direction of the device compared to non-wetting surfaces [57]. Therefore, before the fabrication of complete solar cells using solution processing, we first characterize the Al and Al/MoO_3 electrodes' surface properties. Contact angles (CA) of water and CH_2I_2 on Al and Al/MoO_3 electrodes modified by MoO_3 (30 nm) were measured and the results are shown in Fig. 1(b–e), Fig. 1 (a) shows a schematic diagram of the contact angle. The contact angle of water on the bare Al surface is as large as 79.8° but only 34.4° on the Al/MoO_3 surface. Similar phenomenon was also found for the contact angles of CH_2I_2 on the Al and Al/MoO_3 electrodes, where the contact angles decreased from 26.3° on the bare Al to 15.6° on the Al/MoO_3 electrode. This result reveals that surface modification of Al with MoO_3 could enhance the wettability both for the polar and nonpolar solvent, which would be beneficial for the deposition of organic functional layers.

We perform the Young's equation to calculate the surface energy of a solid surface [58]:

$$(\gamma_s^d \gamma_l^d)^{0.5} + (\gamma_s^p \gamma_l^p)^{0.5} = 0.5\gamma_l(1+\cos\theta) \tag{1}$$

$$\gamma_s = \gamma_s^p + \gamma_s^d \tag{2}$$

Where, γ_s^d and γ_s^p are the dispersion and polarity components of the solid surface energy, γ_l is the liquid surface tension, γ_l^d and γ_l^p are the dispersion and polarity components of the liquid surface tension which has been reported [59], θ is the contact angle between the liquid and solid surface. Contact angles of water and CH_2I_2 on Al/MoO_3 and bare Al

electrode are shown in Fig. 1, and the corresponding solid surface energy γ_s could be calculated according to equation (1). The results are listed in Table 1. As seen here, Al/MoO_3 surface energy is 68.6 mN m⁻¹, much higher than that of Al (46.7 mN m⁻¹). Low surface energy is more suitable for the deposition of PTAA, theoretically, but for a given solid surface, the surface energy has a relationship with its wettability (higher surface energy causes increased wettability) [60]. Although Al surface has relatively lower surface energy to Al/MoO_3 surface, it also corresponds to inappropriate wettability for the deposition of PTAA. The insert of MoO_3 significantly increased the surface energy and also enhanced the surface hydrophilicity, make this surface more suitable for the deposition of subsequent films than bare Al interface.

To clarify that surface modification of the Al electrode with MoO_3 is able to improve the interfacial connection between the organic layer and the electrode, hole-only devices with structures of Al/PTAA (100 nm)/t-MoO_3 (30 nm)/Al (Device A) and Al (100 nm)/b-MoO_3 (30 nm)/PTAA (100 nm)/t-MoO_3 (30 nm)/Al (Device B, Fig. 2a) are fabricated, where 100 nm PTAA was spin-coated on the Al or Al/MoO_3 substrates and both the bottom- (b-MoO_3) and top-MoO_3 (t-MoO_3) layers were deposited by vacuum thermal evaporation. PTAA was chosen as the hole transporting layer since it is widely used in perovskite solar cells. Fig. 2b depicts the current density-voltage (J-V) characters of these two hole-only devices measured at room temperature. As can be seen here, the device A without a bottom MoO_3 layer showed a current density of 3.90 mA cm⁻² at a negative bias of −3.5 V and 0.39 mA cm⁻² at a positive bias of 3.5 V. The unsymmetrical J-V characteristics of device A suggests that a high charge injection barrier exists at the PTAA/Al interface [61]. To quantitatively analyze the hole injection barrier at the PTAA/Al interface, temperature dependent J-V characters of device A were measured and the results are ploted in Fig. 2c according to equations (3) and (4) [62]:

$$\frac{\partial \ln J}{\partial T^{-1}} = \frac{-\varphi + \beta F^{1/2}}{k} \tag{3}$$

$$\beta^2 = q^3/4\pi\varepsilon \tag{4}$$

where the J values were taken from the measured current density at V_{bias} = −3 V under different operating temperatures (T). k is the Boltzmann constant, F is the electric field strength, q is the elementary electronic charge and ε is the polymer dielectric constant. As can be seen from

Table 1
Contact angles on bare Al and Al/MoO_3 surfaces and their surface energy values.

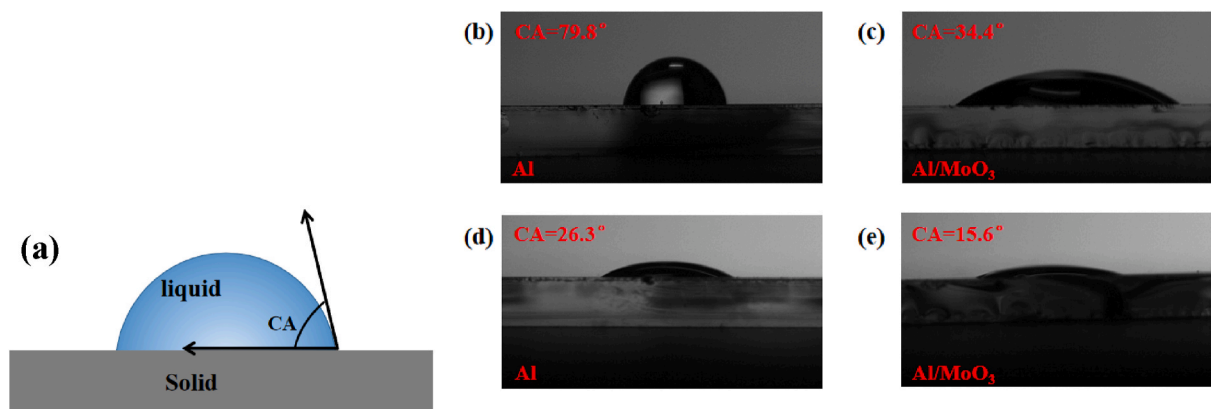| Films	Contact angles (°)		Surface energy (mN m⁻¹)		
	Water	CH_2I_2	γ_s^d	γ_s^p	γ_s
Al	79.8	34.4	44.0	2.7	46.7
Al/MoO_3	26.3	15.6	45.4	23.2	68.6

Fig. 1. (a) A schematic diagram of contact angle and the Contact angles of water (b,c) and CH_2I_2 (d,e) on Al (b,d) and Al/MoO_3 (c,e) surfaces.
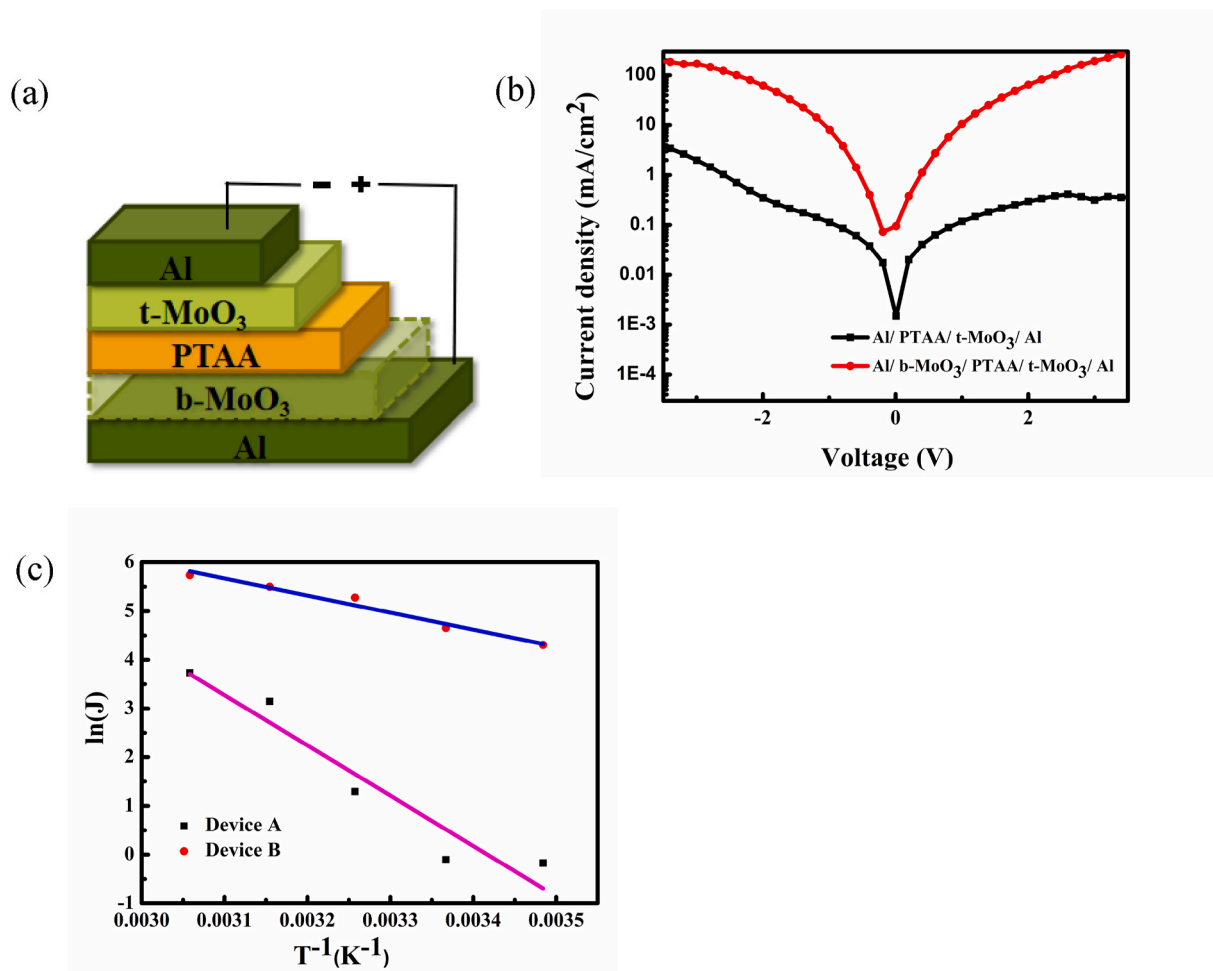
Fig. 2. (a) The hole-only devices with and without b-MoO$_3$ modified structures; (b) J-V characters of these two hole only devices; (c) temperature depended current density at V = -3 V for these two hole only devices.

Fig. 2c, $\frac{\partial \ln J}{\partial T^{-1}}$ could be obtained from the slope of the line fitted to the corresponding data which value is −10328.7, leading to $\varphi = 1.01$ eV. This huge interface barrier height causes the charge to be unable to conduct effectively in the sample with this structure.

In contrast, almost two orders of magnitude enhancement were measured for the device B with the bottom MoO$_3$ layer. High current densities of 198.1 and 265.7 mA cm^{-2} were measured when the device was operated at −3.5 and 3.5 V bias, respectively, suggesting improved interfacial contact at both electrodes. The temperature dependent *J-V* characters of device B has also been investigated and a slope of −3656.2 with a much lower $\varphi = 0.42$ eV of device B could be obtained from Fig. 2 (c), indicating that charge can effectively transfer in this structure and the interface energy barrier is significantly reduced. In other words, the introduction of MoO$_3$ on Al surface will greatly improve the connection between PTAA and Al, which could be originated from two different effects, one is the improved wettability of PTAA on Al surface, and the other one is reduced energy barrier for hole injection. Several findings have shown that charges could hop from an organic semiconductor HOMO level into MoO$_3$, thus the hole-injection barrier at anode/organic interface could be significantly decreased by introducing a MoO$_3$ layer between anode and organic semiconductor [63,64]. Herein, the decreased energy barrier at Al/MoO$_3$/PTAA is believed to be a result of favourable energy-level alignment between MoO$_3$ and PTAA molecules, which is largely influenced by the WF of MoO$_3$.

3.2. Characteristics of perovskite films on different substrates

It is known that the morphology of the perovskite film is highly important for achieving high photovoltaic performance. We then exploit the effect of inserting MoO$_3$ layer between Al and PTAA on the morphology and optoelectronic properties of the perovskite layer. Owing to the poor wettability of perovskite precursor solution on PTAA surface, an additional thin PEI layer was deposited onto the PTAA surface before depositing the perovskite precursor solution [65]. Fig. 3 depicts the scanning electron microscopy (SEM) images of perovskite film deposited on Al/b-MoO$_3$/PTAA and Al/PTAA. For comparison, SEM images of perovskite film on ITO/PTAA was also measured and listed in this Figure. As can be seen here, all these perovskite films deposited on different substrates show homogeneous, pinhole-free, and condense morphology. The crystal sizes are calculated to be 180–270 nm, indicating good film-forming capability on PTAA/PEI surface. In addition to the perovskite crystalline domains, PbI$_2$ phases were also measured in these films as bright phases, which was reported to be beneficial for the high open-circuit voltage (V$_{OC}$) of the cells [50].

We also checked the crystalline structure of the perovskite films on different electrodes by X-ray diffraction (XRD), and the results are shown in Fig. 4. Diffraction peaks of 2θ at 14.13°, 28.48° and 31.93° corresponding to the (110), (220) and (310) of the perovskite crystals are clearly seen [50]. No difference in the diffraction peak position and intensity was found, indicating that perovskite films deposited on Al or ITO substrates have similar crystallinity. Again, weak peaks of 12.65° can be found on all these films, which could be assigned to the formation
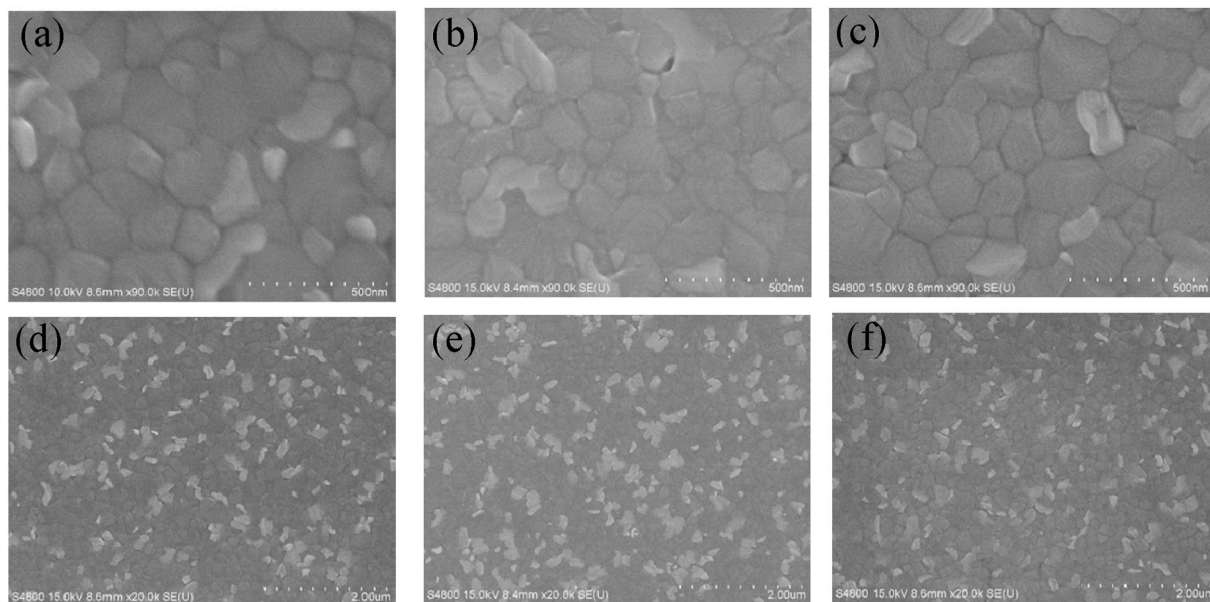
Fig. 3. SEM images of perovskite films deposited on (a, d) ITO/PTAA, (b, e) Al/PTAA and (c, f) Al/b-MoO$_3$/PTAA under local scans (a, b, c) and large area scans (d, e, f).
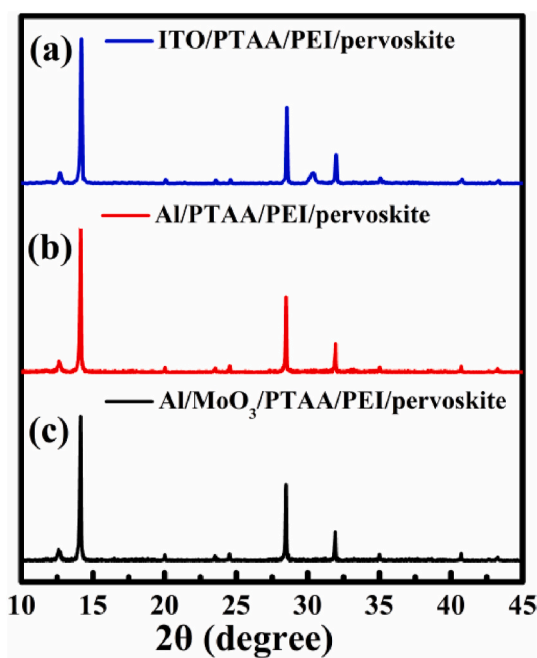

Fig. 4. The XRD patterns of perovskite films deposited on PTAA/PEI on different electrode.

of PbI$_2$ crystals, in good consistent with SEM results. Nevertheless, no significant difference was found for the perovskite films deposited on the different electrodes, the final device performance should not be due to the difference on the perovskite thin film morphology (*vide infra*).

3.3. Perovskite solar cells with thermal evaporated silver thin film top electrode

We then fabricated and tested inverted perovskite solar cells based on Al or Al/MoO$_3$ bottom electrode. For comparison, perovskite solar cells with ITO bottom electrode were also fabricated and tested. In this set of experiments, we used thermal evaporated 12 nm Ag thin film as

the transparent top electrode [30]. Although low averaged visible (400–800 nm) light transparence (AVT) of 26.5% was measured for the 12 nm Ag thin film electrode (Fig. 5c), deposition of the Ag electrode via thermal evaporation can minimize the uncertain influence of organic solvent when spray coating the AgNW electrode and therefore is better for the study of the influence of the bottom electrode on the perovskite solar cell performance.

We first compare the photovoltaic performance of the perovskite solar cells on Al and ITO bottom electrode directly. Fig. 5a and b depict the device structure and band alignment diagram of the perovskite solar cells, respectively. Fig. 5c shows the transmittance of the ITO and e-Ag electrode. For the ITO-based cell (with a structure of ITO/PTAA//PEI/ perovskite/PC$_{61}$BM/PEI/e-Ag, Device 1), since both electrodes are transparent, we checked the cell's photovoltaic performance illuminated from either ITO or e-Ag side. For the Al bottom electrode-based cell (with a structure of Al/PTAA//PEI/perovskite/PC$_{61}$BM/PEI/e-Ag, Device 2), we only check the photovoltaic perovskite cell illuminated from the e-Ag top electrode. The J-V characters of these cells are shown in Fig. 5d, and the photovoltaic performance data are summarized in Table 2. As seen from here, the Device 1 illuminated from the ITO side showed a high V_{oc} of 1.09 V, a short-circuit current (J_{sc}) of 20.62 mA cm^{-2}, a fill factor (FF) of 0.71, and an overall PCE of 16.00%, which is comparable with the semitransparent perovskite cell reported in the literature [46]. When the cell is illuminated from the e-Ag side, a V_{oc} of 1.03 V, a J_{sc} of 3.91 mA cm^{-2}, an FF of 0.72, and a PCE of 2.90% was measured, which is much lower than illuminated from the ITO side. This is mainly due to the lowered J_{sc} originating from the low light transparency of the e-Ag electrode (Fig. 5c). Nevertheless, the results of the ITO based cell suggest that all the functional layers within the cell are well interconnected. In contrast, the PVSK cell based on the bare Al bottom electrode (Device 2) shows a poor performance with a V_{oc} of 0.60 V, extremely low J_{sc} (0.05 mA cm^{-2}) and FF (0.14), resulting in a low PCE of 0.004%. Except for the bottom electrode, the ITO and Al based cells have identical layer stacking structure. The low performance of the Al based cell is then attributed to the unsatisfied interfacial connection between Al and PTAA (*vide supra*).

Thin MoO$_3$ layer with different thicknesses (15, 30, and 40 nm) was then inserted in between Al bottom electrode and PTAA layer. Fig. 5e shows the J-V curves of the cells and the photovoltaic performance data are listed in Table 2 for comparison. As reported, the MoO$_3$ work
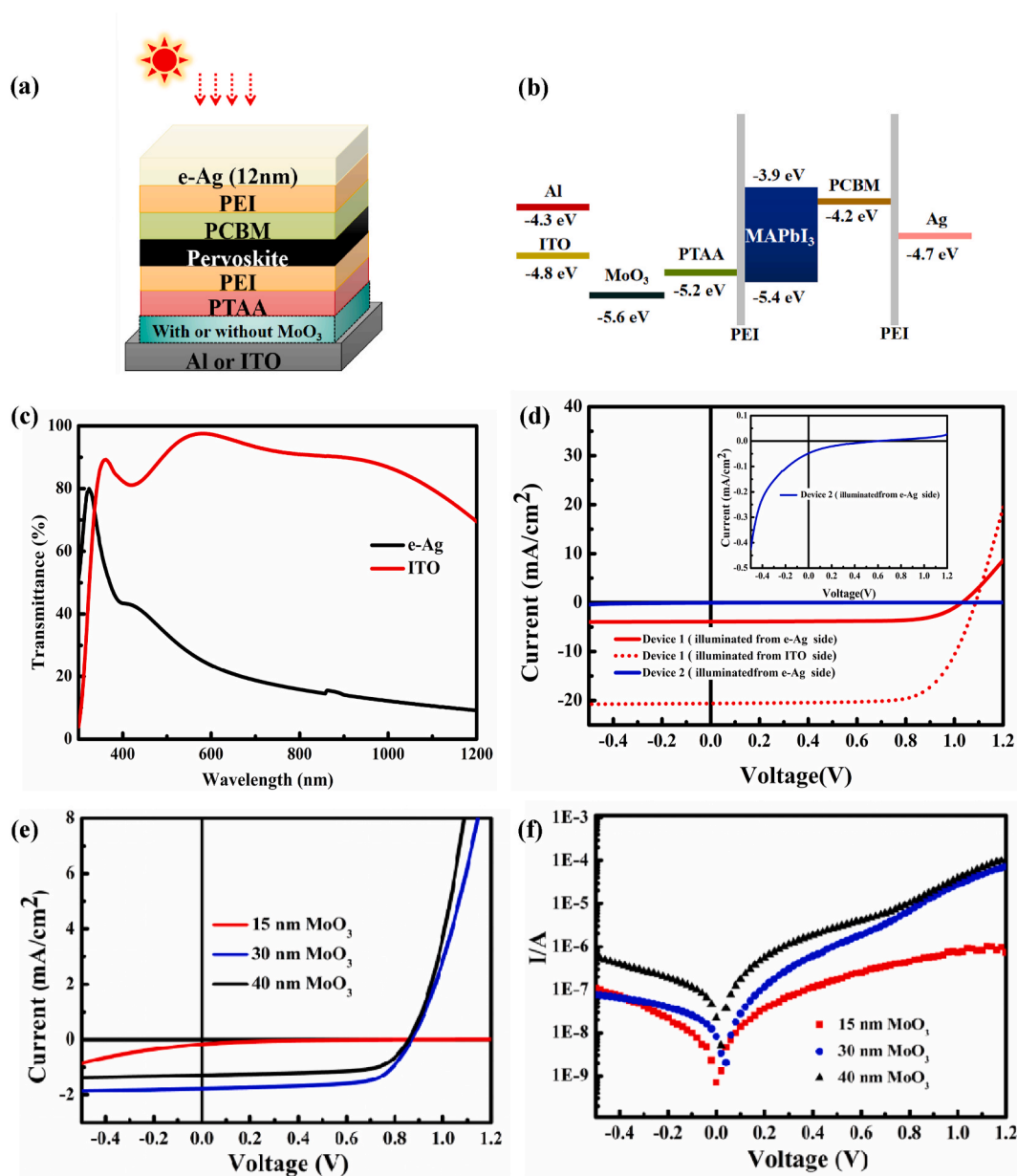
Fig. 5. (a) Device structure and (b) band alignment diagram of PVSKs based on Al and ITO bottom electrodes. (c) The transmittance of bare ITO and e-Ag electrodes. (d) *J-V* curves of Device 1 and Device 2, the zoom in figure shows the photovoltaic property of Device 2. Light (e) and dark (f) currents of Al based devices with different MoO$_3$ interfacial layer, respectively.

Table 2
The photovoltaic properties of perovskite solar cells based on ITO, Al, or Al/MoO$_3$ electrode with thermal evaporated thin Ag electrode (12 nm).

Bottom Electrode	*Voc* (V)	*Jsc* (mA cm^{-2})	FF	PCE (%)
ITO (ITO side)	1.09	20.62	0.71	16.00
ITO (e-Ag side)	1.03	3.91	0.72	2.90
Al	0.60	0.05	0.14	0.004
Al/MoO$_3$ (15 nm)	0.65	0.05	0.15	0.01
Al/MoO$_3$ (30 nm)	0.87	1.76	0.67	1.03
Al/MoO$_3$ (40 nm)	0.86	1.28	0.67	0.74

function and electronic band structure are related to the film thickness [66]. When the MoO$_3$ layer is too thin (15 nm) to realize interfacial connection between Al and PTAA layer, the cell shows still very poor performance with extremely low *J*sc. However, when the MoO$_3$ layer is increased to 30 nm, the perovskite cell showed a *J*sc of 1.76 mA cm^{-2}

with a *Voc* of 0.87 V, an FF of 0.67 and an overall PCE of 1.03% (Fig. 5e). Although the cell performance is still low, this result confirmed that the insertion of 30 nm MoO$_3$ layer is able to improve the connection between Al electrode and PTAA layer and consequently improve the device performance. Further increase of the thickness of MoO$_3$ layer (40 nm), however, lowers the device performance, which could be owing to the reduced electron blocking property of the thick MoO$_3$ layer, as seen from the dark J-V characteristics.

The improvement of the interfacial connection between Al and PTAA layer was also confirmed by the dark *J-V* characteristics of the cells (Fig. 5f). Very low current density was measured for the cell with 15 nm MoO$_3$ thin film (similar to that of MoO$_3$-free cell), indicating a large hole injection barrier at the Al/PTAA interface. Increasing the layer thickness of MoO$_3$ to 30 nm, larger current was measured with a high rectification coefficient. Interestingly, further increase of the MoO$_3$ layer thickness to 40 nm, large dark saturated current was measured, indicating a worse electron blocking capability of the thick MoO$_3$ layer, which can be

understood by the n-type characteristics of MoO$_3$ [64].

3.4. Perovskite solar cells with spray-coated silver nanowire top electrode

Knowing that AgNWs have balanced conductivity and light transparency, to improve further the performance of PVSK based on opaque Al electrode, we used a spray-coated AgNW electrode as the top transparent electrode. To protect the AgNW electrode from the chemical corrosion of perovskite material and to improve the interface connection of PC$_{61}$BM with AgNW electrode, a thin layer of PEI was deposited onto the PC$_{61}$BM before spray-coating AgNW layer. The concentration and spray-coating processes were optimized, and a highly transparent AgNWs conductive film with a sheet resistance of 27.0 Ω □$^{-1}$ and a light transparency of 92% at 550 nm was achieved, which showed 3 times higher the transmittance than the 12 nm e-Ag film. Finally, perovskite solar cell based on opaque Al electrode with a structure of Al/MoO$_3$ (30 nm)/PTAA/PEI/perovskite/PC$_{61}$BM/PEI/AgNWs was fabricated (Fig. 6a). For comparison, semitransparent PVSK with a transparent ITO bottom electrode were also fabricated. Fig. 6b and c showed the *J–V* characteristic curves and EQE spectra of the best performance cells, and the photovoltaic performance data are summarized in Table 3. As seen here, the AgNW based perovskite solar cell showed a *Voc* of 1.07 V, a *Jsc* of 19.95 mA cm^{-2}, an FF of 0.42, and a PCE of 7.09%, which is almost 7 times that of the e-Ag based cell. Similar photovoltaic performance was obtained for the ITO based cell (Table 3), indicating that hole injection efficiency at the PTAA/MoO$_3$/Al is comparable to the PTAA/ITO interface. It worth noting that both cells showed low FF around 0.40, which is owing to the high series resistance of the cell (Table 3). This can be ascribed to a non-ideal interface connection at the PC$_{61}$BM/PEI/AgNW interface. Further optimization of the cell structure is undergoing. The EQE spectrum of Al/MoO$_3$ based cell showed slightly lower

Table 3
The photovoltaic properties of the best performance perovskite solar cells based on Al and ITO bottom electrodes.

	Voc (V)	Jsc (mA cm^{-2})	FF	PCE (%)	R$_s$(Ω*cm^2)	R$_{sh}$(Ω*cm^2)
Al/MoO$_3$ (AgNW side)	1.07	15.95	0.42	7.09	35.03	645.90
ITO (ITO side)	1.08	17.29	0.47	8.77	25.57	942.80
ITO (AgNW side)	1.09	16.46	0.44	7.88	35.78	796.89

quantum efficiency at 400–550 nm but higher quantum efficiency at 650–800 nm than that of ITO based cell. When illuminated from AgNWs side, the lower EQE at short wavelength range of both ITO and Al based devices can be ascribed to the light absorption and reflection of the AgNW electrode. At long wavelength range, the higher EQE observed at Al based cell can be ascribed to the light reflection effect of Al electrode, confirming that using opaque Al electrode is helpful in achieving higher light unitization.

Opaque metal act as bottom electrode has the advantage of reducing the production cost of perovskite solar cells. In the previous reports, Al has the risk to react with the mobile ions from halide perovskite which degrades the perovskite photovoltaics performance [67,68]. Therefore, introducing a dense functional layer between Al and perovskite which reduces the migration of metal ions is necessary. In order to further enhance the performance of this kind of perovskite solar cells, combined with the results provided in this report, we think further research could focus on the following two aspects: 1) Further improve the connection between metal bottom electrode and upper charge transport layer, minimum the interface energy barrier would be beneficial to enhance
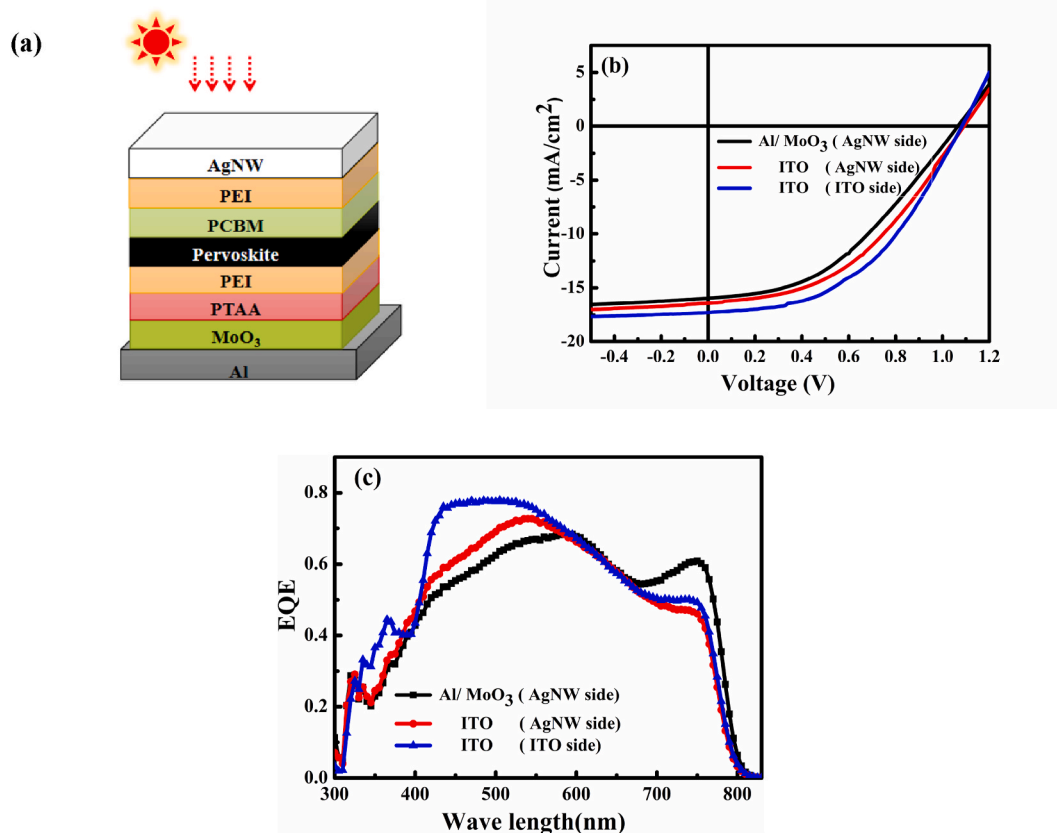

Fig. 6. (a) Device structure of perovskite solar cells based on Al bottom electrode with spray-coated AgNW as top electrode. (b) *J-V* curves and (c) EQE spectra of the best performance devices based on Al and ITO bottom electrodes, ITO bottom electrode device has been tested from both ITO and AgNW side.

the PCE of perovskite solar cells based on opaque metal bottom electrode. 2) The opacity of the metal bottom electrode means that this kind of device should illuminated from top electrode side, thus high quality transparent conductive electrodes with high conductivity, transmittance as well as suitable preparation method should be investigated.

4. Conclusions

In summary, we have successfully fabricated perovskite solar cell on opaque Al bottom electrode. By inserting a thin MoO_3 layer between Al and upper hole transport layer, the mismatched work function of the interfaces could be minimized, resulting in much enhanced hole injection and extraction efficiency. By using spray-coating silver nanowire networks as the transparent top electrode, an ITO free perovskite solar cell with a power conversion efficiency of 7.09% was achieved. This work has provided an implementation simplicity and cost-saving alternative to instead of traditional high-cost ITO electrode that further promotes the perovskite solar cell preparation cost reduction.

Declaration of competing interest

The authors declare that they have no known competing financial interests or personal relationships that could have appeared to influence the work reported in this paper.

References

[1] A. Kojimar, K. Teshima, Y. Shirai, T. Miyasaka, Organometal halide perovskites as visible-light sensitizers for photovoltaic cells, J. Am. Chem. Soc. 131 (2009) 6050–6051.
[2] National Renewable Energy Laboratory (NREL), Best research-cell efficiency chart. https://www.nrel.gov/pv/cell-efciency.htmll. (Accessed January 2021).
[3] D.W. Ferdani, S.R. Pering, D. Ghosh, P. Kubiak, A.B. Walker, S.E. Lewis, A.L. Johnson, P.J. Baker, M.S. Islam, P.J. Cameron, Partial cation substitution reduces iodide ion transport in lead iodide perovskite solar cells, Energy Environ. Sci. 12 (2019) 2264–2272.
[4] T. Du, C.H. Burgess, C.T. Lin, F. Eisner, J. Kim, S. Xu, H. Kang, J.R. Durrant, M.A. McLachlan, Probing and controlling intragrain crystallinity for improved low temperature–processed perovskite solar cells, Adv. Funct. Mater. 28 (2018) 1803943.
[5] J.P. Correa-Baena, A. Abate, M. Saliba, W. Tress, T.J. Jacobsson, M. Grätzel, A. Hagfeldt, The rapid evolution of highly efficient perovskite solar cells, Energy Environ. Sci. 10 (2017) 710–727.
[6] H. Lu, X. Ren, D. Ouyang, W.C. Choy, Emerging novel metal electrodes for photovoltaic applications, Small 14 (2018) 1703140.
[7] T. Putnin, C. Lertvachirapaiboon, R. Ishikawa, K. Shinbo, K. Kato, S. Ekgasit, K. Ounnunkad, A. Baba, Enhanced organic solar cell performance: multiple surface plasmon resonance and incorporation of silver nanodisks into a grating-structure electrode, Opto-Electron. Adv. 2 (2019) 190010.
[8] S. Honey, J. Asim, I. Ahmad, T. Zhao, M. Maaza, Modification in properties of Ni-NWs meshes by Ar+ ions beam irradiation, Mater. Res. Express 7 (2020) 65008.
[9] H. Sung, N. Ahn, M.S. Jang, J.K. Lee, H. Yoon, N.G. Park, M. Choi, Transparent conductive oxide-free graphene-based perovskite solar cells with over 17% efficiency, Adv. Energy Mater. 6 (2016) 1501873.
[10] M. Batmunkh, C.J. Shearer, M.J. Biggs, J.G. Shapter, Solution processed graphene structures for perovskite solar cells, J. Mater. Chem. 4 (2016) 2605–2616.
[11] J. Yoon, H. Sung, G. Lee, W. Cho, N. Ahn, H.S. Jung, M. Choi, Superflexible high-efficiency perovskite solar cells utilizing graphene electrodes: towards future foldable power sources, Energy Environ. Sci. 10 (2017) 337–345.
[12] S. Albrecht, M. Saliba, J.P.C. Baena, F. Lang, L. Kegelmann, M. Mews, L. Steier, A. Abate, J. Rappich, L. Korte, Monolithic perovskite/silicon-heterojunction tandem solar cells processed at low temperature, Energy Environ. Sci. 9 (2016) 81–88.
[13] K.A. Bush, C.D. Bailie, Y. Chen, A.R. Bowring, W. Wang, W. Ma, T. Leijtens, F. Moghadam, M.D. McGehee, Thermal and environmental stability of semitransparent perovskite solar cells for tandems enabled by a solution-processed nanoparticle buffer layer and sputtered ITO electrode, Adv. Mater. 28 (2016) 3937–3943.

[14] J.H. Heo, H.J. Han, M. Lee, M. Song, D.H. Kim, S.H. Im, Stable semitransparent CH3NH3PbI3 planar sandwich solar cells, Energy Environ. Sci. 8 (2015) 2922–2927.
[15] X.L. Ou, M. Xu, J. Feng, H.B. Sun, Flexible and efficient ITO-free semitransparent perovskite solar cells, Sol. Energy Mater. Sol. Cell. 157 (2016) 660–665.
[16] N.L. Chang, A.W. Yi Ho-Baillie, P.A. Basore, T.L. Young, R. Evans, R.J. Egan, A manufacturing cost estimation method with uncertainty analysis and its application to perovskite on glass photovoltaic modules, Prog. Photovoltaics Res. Appl. 25 (2017) 390–405.
[17] Z. Li, S.A. Kulkarni, P.P. Boix, E. Shi, A. Cao, K. Fu, S.K. Batabyal, J. Zhang, Q. Xiong, L.H. Wong, Laminated carbon nanotube networks for metal electrode-free efficient perovskite solar cells, ACS Nano 8 (2014) 6797–6804.
[18] P. You, Z. Liu, Q. Tai, S. Liu, F. Yan, Efficient semitransparent perovskite solar cells with graphene electrodes, Adv. Mater. 27 (2015) 3632–3638.
[19] Z. Ku, Y. Rong, M. Xu, T. Liu, H. Han, Full printable processed mesoscopic CH3NH3PbI3/TiO2 heterojunction solar cells with carbon counter electrode, Sci. Rep. 3 (2013) 1–5.
[20] H. Wei, J. Xiao, Y. Yang, S. Lv, J. Shi, X. Xu, J. Dong, Y. Luo, D. Li, Q. Meng, Free-standing flexible carbon electrode for highly efficient hole-conductor-free perovskite solar cells, Carbon 93 (2015) 861–868.
[21] F. Jiang, T. Liu, S. Zeng, Q. Zhao, X. Min, Z. Li, J. Tong, W. Meng, S. Xiong, Y. Zhou, Metal electrode-free perovskite solar cells with transfer-laminated conducting polymer electrode, Opt Express 23 (2015) A83–A91.
[22] L. Bu, Z. Liu, M. Zhang, W. Li, A. Zhu, F. Cai, Z. Zhao, Y. Zhou, Semitransparent fully air processed perovskite solar cells, Acs Appl Mater Inter 7 (2015) 17776–17781.
[23] X. Hu, Z. Huang, X. Zhou, P. Li, Y. Wang, Z. Huang, M. Su, W. Ren, F. Li, M. Li, Wearable large-scale perovskite solar-power source via nanocellular scaffold, Adv. Mater. 29 (2017) 1703236.
[24] B.A. Nejand, P. Nazari, S. Gharibzadeh, V. Ahmadi, A. Moshaii, All-inorganic large-area low-cost and durable flexible perovskite solar cells using copper foil as a substrate, Chem. Commun. 53 (2017) 747–750.
[25] G.S. Han, S. Lee, M.L. Duff, F. Qin, J.K. Lee, Highly bendable flexible perovskite solar cells on a nanoscale surface oxide layer of titanium metal plates, Acs Appl Mater Inter 10 (2018) 4697–4704.
[26] J.P. Mailoa, C.D. Bailie, E.C. Johlin, E.T. Hoke, A.J. Akey, W.H. Nguyen, M.D. McGehee, T. Buonassisi, A 2-terminal perovskite/silicon multijunction solar cell enabled by a silicon tunnel junction, Appl. Phys. Lett. 106 (2015) 121105.
[27] F. Guo, H. Azimi, Y. Hou, T. Przybilla, M. Hu, C. Bronnbauer, S. Langner, E. Spiecker, K. Forberich, C.J. Brabec, High-performance semitransparent perovskite solar cells with solution-processed silver nanowires as top electrodes, Nanoscale 7 (2015) 1642–1649.
[28] L. Qiu, J. Deng, X. Lu, Z. Yang, H. Peng, Integrating perovskite solar cells into a flexible fiber, Angew. Chem. Int. Ed. 53 (2014) 10425–10428.
[29] X. Wang, Z. Li, W. Xu, S.A. Kulkarni, S.K. Batabyal, S. Zhang, A. Cao, L.H. Wong, TiO2 nanotube arrays based flexible perovskite solar cells with transparent carbon nanotube electrode, Nano Energy 11 (2015) 728–735.
[30] M. Lee, Y. Jo, D.S. Kim, Y. Jun, Flexible organo-metal halide perovskite solar cells on a Ti metal substrate, J. Mater. Chem. 3 (2015) 4129–4133.
[31] J. Troughton, D. Bryant, K. Wojciechowski, M.J. Carnie, H. Snaith, D.A. Worsley, T.M. Watson, Highly efficient, flexible, indium-free perovskite solar cells employing metallic substrates, J. Mater. Chem. 3 (2015) 9141–9145.
[32] M. Lee, Y. Jo, D.S. Kim, H.Y. Jeong, Y. Jun, Efficient, durable and flexible perovskite photovoltaic devices with Ag-embedded ITO as the top electrode on a metal substrate, J. Mater. Chem. 3 (2015) 14592–14597.
[33] M. Lee, Y. Ko, B.K. Min, Y. Jun, Silver nanowire top electrodes in flexible perovskite solar cells using titanium metal as substrate, ChemSusChem 9 (2016) 31–35.
[34] Y. Xiao, G. Han, H. Zhou, J. Wu, An efficient titanium foil based perovskite solar cell: using a titanium dioxide nanowire array anode and transparent poly (3, 4-ethylenedioxythiophene) electrode, RSC Adv. 6 (2016) 2778–2784.
[35] F. Qin, J. Tong, R. Ge, B. Luo, F. Jiang, T. Liu, Y. Jiang, Z. Xu, L. Mao, W. Meng, Indium tin oxide (ITO)-free, top-illuminated, flexible perovskite solar cells, J. Mater. Chem. 4 (2016) 14017–14024.
[36] C. Hanmandlu, C.C. Liu, C.Y. Chen, K.M. Boopathi, S.H. Wu, M. Singh, A. Mohapatra, H.W. Lin, Y.C. Chang, Y.C. Chang, Top illuminated hysteresis-free perovskite solar cells incorporating microcavity structures on metal electrodes: a combined experimental and theoretical approach, Acs Appl Mater Inter 10 (2018) 17973–17984.
[37] H.B. Michaelson, The work function of the elements and its periodicity, J. Appl. Phys. 48 (1977) 4729–4733.
[38] J. Wang, F. Fei, Q. Luo, S. Nie, N. Wu, X. Chen, W. Su, Y. Li, C.Q. Ma, Modification of the highly conductive PEDOT: PSS layer for use in silver nanogrid electrodes for flexible inverted polymer solar cells, Acs Appl Mater Inter 9 (2017) 7834–7842.
[39] Y. Zhang, X. Liu, H. Gu, L. Yan, H. Tan, C.Q. Ma, Y. Lin, Cyclopentadithiophene cored A-π-D-π-A non-fullerene electron acceptor in ternary polymer solar cells to extend the light absorption up to 900 nm, Org. Electron. 77 (2020) 105530.
[40] L. Yan, J. Yi, Q. Chen, J. Dou, Y. Yang, X. Liu, L. Chen, C.Q. Ma, External load-dependent degradation of P3HT: PC61BM solar cells: behavior, mechanism, and method of suppression, J. Mater. Chem. 5 (2017) 10010–10020.
[41] Q. Chen, L. Yuan, R. Duan, P. Huang, J. Fu, H. Ma, X. Wang, Y. Zhou, B. Song, Zwitterionic polymer: a facile interfacial material works at both anode and cathode in p-i-n perovskite solar cells, Sol. Rrl. 3 (2019) 1900118.
[42] Y. Zhao, A.M. Nardes, K. Zhu, Effective hole extraction using MoOx-Al contact in perovskite CH3NH3PbI3 solar cells, Appl. Phys. Lett. 104 (2014) 213906.

[43] Y. Shao, Y. Yuan, J. Huang, Correlation of energy disorder and open-circuit voltage in hybrid perovskite solar cells, Nat. Energy 1 (2016) 1–6.

[44] H. Lu, J. Lin, N. Wu, S.H. Nie, Q. Luo, C.Q. Ma, Z. Cui, Inkjet printed silver nanowire network as top electrode for semi-transparent organic photovoltaic devices, Appl. Phys. Lett. 106 (2015), 093302.

[45] G.Q. Ji, Y.L. Wang, Q. Luo, K. Han, M.L. Xie, L.P. Zhang, N. Wu, J. Lin, S.G. Xiao, Y. Q. Li, L.Q. Luo, C.Q. Ma, Fully coated semitransparent organic solar cells with a doctor-blade-coated composite anode buffer layer of phosphomolybdic acid and PEDOT: PSS and a spray-coated silver nanowire top electrode, ACS Appl. Mater. Interfaces 10 (2018) 943–954.

[46] M.L. Xie, H. Lu, L.P. Zhang, J. Wang, Q. Luo, J. Lin, L.X. Ba, H. Liu, W.Z. Shen, L. Y. Shi, C.Q. Ma, Fully solution-processed semi-transparent perovskite solar cells with ink-jet printed silver nanowires top electrode, Sol. Rrl. 2 (2018) 1770152.

[47] K. Han, M.L. Xie, L.P. Zhang, L.P. Yan, J.F. Wei, G.Q. Ji, Q. Luo, J. Lin, Y.Y. Hao, C. Q. Ma, Fully solution processed semitransparent perovskite solar cells with spray-coated silver nanowires/ZnO composite top electrode, Sol. Energy Mater. Sol. Cell. 185 (2018) 399–405.

[48] N.J. Jeon, J.H. Noh, Y.C. Kim, W.S. Yang, S. Ryu, S.I. Seok, Solvent engineering for high-performance inorganic–organic hybrid perovskite solar cells, Nat. Mater. 13 (2014) 897–903.

[49] Y.C. Shao, Z.G. Xiao, C. Bi, Y.B. Yuan, J.S. Huang, Origin and elimination of photocurrent hysteresis by fullerene passivation in $CH_3NH_3PbI_3$ planar heterojunction solar cells, Nat. Commun. 5 (2014) 1–7.

[50] M.X. Tan, G.Q. Ji, L.P. Zhang, J. Wang, C. Wang, Q. Chen, Q. Luo, L.W. Chen, C. Q. Ma, Simultaneous performance and stability improvement of perovskite solar cells by a sequential twice anti-solvent deposition process, Org. Electron. 59 (2018) 358–365.

[51] K.C. Wang, P.S. Shen, M.H. Li, S. Chen, M.W. Lin, P. Chen, T.F. Guo, Low-temperature sputtered nickel oxide compact thin film as effective electron blocking layer for mesoscopic $NiO/CH_3NH_3PbI_3$ perovskite heterojunction solar cells, Acs Appl Mater Inter 6 (2014) 11851–11858.

[52] K.C. Wang, J.Y. Jeng, P.S. Shen, Y.C. Chang, E.W.G. Diau, C.H. Tsai, T.Y. Chao, H. C. Hsu, P.Y. Lin, P. Chen, P-type mesoscopic nickel oxide/organometallic perovskite heterojunction solar cells, Sci. Rep. 4 (2014) 1–8.

[53] P. Da, G. Zheng, Tailoring interface of lead-halide perovskite solar cells, Nano Res. 10 (2017) 1471–1497.

[54] C. Liu, Y. Xu, Y.Y. Noh, Contact engineering in organic field-effect transistors, Mater. Today 18 (2015) 79–96.

[55] J. Meyer, R. Khalandovsky, P. Görrn, A. Kahn, MoO_3 films spin-coated from a nanoparticle suspension for efficient hole-injection in organic electronics, Adv. Mater. 23 (2011) 70–73.

[56] D. Kumaki, T. Umeda, S. Tokito, Reducing the contact resistance of bottom-contact pentacene thin-film transistors by employing a MoOx carrier injection layer, Appl. Phys. Lett. 92 (2008), 013301.

[57] C. Liu, W. Li, J. Chen, J. Fan, Y. Mai, R.E. Schropp, Ultra-thin MoOx as cathode buffer layer for the improvement of all-inorganic $CsPbIBr_2$ perovskite solar cells, Nano Energy 41 (2017) 75–83.

[58] I. Irfan, J.F. Wei, X. Sun, W.S. Zha, M. Khalil, L.P. Zhang, R. Huang, Z.J. Chen, Y. B. Shen, F.S. Li, Q. Luo, C.Q. Ma, Simultaneous improvement of the long-term and thermal stability of the perovskite solar cells using 2,3,4,5,6-pentafluorobenzoyl chloride (PFBC)-Capped ZnO nanoparticles buffer layer, Inside Solaris R 4 (2020) 2000289.

[59] W.H. Ming, L. van Ravenstein, R. van Grampel, W. van Gennip, M. Krupers, H. Niemantsverdriet, R. Linde, van der, Low surface energy polymeric films from partially fluorinated photocurable solventless liquid oligoesters, Polym. Bull. 47 (2001) 321–328.

[60] A.P.S. Gaur, S. Sahoo, M. Ahmadi, S.P. Dash, M.J.F. Guinel, R.S. Katiyar, Surface energy engineering for tunable wettability through controlled synthesis of MoS_2, Nano Lett. 14 (2014) 4314–4321.

[61] N.B. Kotadiya, H. Lu, A. Mondal, Y. Ie, D. Andrienko, P.W.M. Blom, G.-J.A. H. Wetzelaer, Universal strategy for Ohmic hole injection into organic semiconductors with high ionization energies, Nat. Mater. 17 (2018) 329–334.

[62] D. Ma, I. Hümmelgen, R.W. Li, J. Gruber, Charge injection and transport in poly (4, 4'-biphenylenevinylene), J. Phys. D Appl. Phys. 33 (2000) 1376–1379.

[63] M. Kröger, S. Hamwi, J. Meyer, T. Riedl, W. Kowalsky, A. Kahn, Role of the deep-lying electronic states of MoO_3 in the enhancement of hole-injection in organic thin films, Appl. Phys. Lett. 95 (2009) 251.

[64] M.T. Greiner, M.G. Helander, W.M. Tang, Z.B. Wang, J. Qiu, Z.H. Lu, Universal energy-level alignment of molecules on metal oxides, Nat. Mater. 11 (2012) 76–81.

[65] J.F. Wei, Photoelectric Properties of Zinc Oxide-Organic Composite Interface Layer and its Application in Organic Photovoltaics Solar Cells, PhD Dissertation, University of Chinese Academy of Sciences, 2019.

[66] M.T. Greiner, L. Chai, M.G. Helander, W.M. Tang, Z.H. Lu, Metal/metal-oxide interfaces: how metal contacts affect the work function and band structure of MoO_3, Adv. Funct. Mater. 23 (2013) 215–226.

[67] H.H. Ding, B.R. Li, S. Zareen, G.H. Li, Y. Tu, D.L. Zhang, X. Cao, Q. Xu, S.F. Yang, S. L. Tait, J.F. Zhu, In situ investigations of Al/perovskite interfacial structures, ACS Appl. Mater. Interfaces 12 (2020) 28861–28868.

[68] B. Roose, Q. Wang, A. Abate, The role of charge selective contacts in perovskite solar cell stability, Adv. Energy Mater. 9 (2019) 1803140.